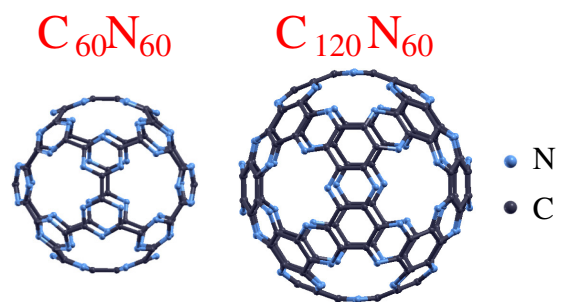


Graphical Abstract

Porous carbon nitride fullerenes: a novel family of porous cage molecules

Zacharias G. Fthenakis, Nektarios N. Lathiotakis



Porous carbon nitride fullerenes: a novel family of porous cage molecules[★]

Zacharias G. Fthenakis^{a,b,c,*}, Nektarios N. Lathiotakis^{a,*}

^aTheoretical and Physical Chemistry Institute, National Hellenic Research Foundation, , Athens, GR-11635, Greece

^bIstituto Nanoscienze-CNR, Piazza San Silvestro 12, Pisa, 56127, Italy

^cNEST, Scuola Normale Superiore, Piazza San Silvestro 12, Pisa, 56127, Italy

ARTICLE INFO

Keywords:

fullerenes
graphitic carbon nitride
porous cage molecules
density functional theory

ABSTRACT

We propose and study theoretically a novel family of cage molecules, the porous carbon nitride fullerenes (PCNFs), which can be considered the zero-dimensional counterparts of the two-dimensional porous graphitic carbon nitrides, in accordance with icosahedral fullerenes, representing the zero-dimensional counterpart of graphene. We focus on two representative members of the PCNF family, the icosahedral $C_{60}N_{60}$ and $C_{120}N_{60}$ which are the first members of the two main sub-families of these structures derived from the class I and II Goldberg polyhedra, respectively. Taking into account that the two-dimensional graphitic carbon nitrides are considered the next-generation materials for several interesting applications, the interest in their zero-dimension counterparts is obvious. In the present study, we utilize Density Functional Theory to find their structural, vibrational, and electronic properties. The stability of the proposed cages was demonstrated through vibrational analysis and molecular dynamics simulations with ReaxFF potentials. Regarding thermal stability, we found that $C_{60}N_{60}$ could be stable well above 1000 K and $C_{120}N_{60}$ well above 2000 K. Finally, we discuss several ideas regarding precursors that could be possibly used for their bottom-up synthesis.

1. Introduction

Given that fullerenes are the zero-dimensional (0D) analogues of graphene, a question that naturally arises is whether 0D fullerene analogues of two-dimensional (2D) porous graphitic carbon nitrides ($g-C_nN_m$) exist.


Porous $g-C_nN_m$ constitute a family of periodic graphene-based structures, incorporating substitutional N atoms in several sites of a porous graphene lattice [1–9]. A pore is formed in the absence of some C atoms of the pure graphene honeycomb lattice, and substitution of the two-fold coordinated C atoms at the pore boundary with N atoms (pyridinic N atoms). Pyridinic N atoms appear entirely at the pore edges, while three-fold coordinated N atoms (graphitic N atoms) may also appear in the structure, substituting three-fold coordinated C atoms. In these structures, N atoms are not favorable in nearest-neighbor lattice positions, since they are repulsive due to their negative charge [10]. Thus, such an arrangement of N atoms does not appear in the structure.

Several structures in the porous $g-C_nN_m$ family have been reportedly synthesized. In the sub-family of structures containing both graphitic and pyridinic nitrogen atoms, representative examples are two distinct $g-C_3N_4$ structures, one consisting of triazine-based [1] and one of heptazine-based [2] units. These structures are predominantly observed in multilayer graphitic-like forms. Another heptazine-based

structure of this sub-family, $g-C_3N_2$, is also reportedly synthesized. [3] In the sub-family of structures with only pyridinic N atoms, notable examples are the $g-C_2N$ [4–7, 9] and $g-CN$ [8, 9]. These structures have attracted considerable scientific interest over the last decade, exhibiting a broad spectrum of applications, which include catalysis [2, 11–20], (such as photocatalytic water splitting [2, 17–19] and single atom catalysis [20]), gas separation [21–27] and nanofiltration [28], water desalination [29], hydrogen storage [30], and anode materials for Li-ion batteries [31]. Given that the 0D counterparts of porous $g-C_nN_m$ s will be structurally very similar to them, it is reasonable to expect that the above interesting properties of porous $g-C_nN_m$ would be inherited by their 0D counterparts. Furthermore, these 0D structures may exhibit additional novel properties due to their specific cage geometry and finite size, including properties arising from quantum confinement. Hence, the elevated interest in them is more than obvious.

Considering that (i) the relation between these 0D fullerene-like structures with porous $g-C_nN_m$ is analogous to the connection between icosahedral fullerenes and graphene, and (ii) the design of porous $g-C_nN_m$ involves the formation of pores and substitution of appropriate C atoms with N atoms, as described above, the form of these molecules can be easily derived from Goldberg polyhedra [32], in a similar way to the design of icosahedral fullerenes. The design of such 0D structures, which we call “porous carbon nitride fullerenes” (PCNFs), needs the formation of proper pores in icosahedral fullerenes in a way that retains full icosahedral symmetry.

Since only $(n, 0)$ and (n, n) Goldberg polyhedra have full icosahedral symmetry [33], the design of a fully icosahedral PCNF implies the introduction of several pores in

 fthenak@eie.gr, zacharias.fthenakis@nano.cnr.it (Z.G.

Fthenakis); lathiot@eie.gr (N.N. Lathiotakis)



<https://www.nano.cnr.it/researcher-profile/zacharias-fthenakis/> (Z.G. Fthenakis);

<http://www.eie.gr/nhrf/institutes/tpci/cvs/cv-lathiotakis-en.pdf> (N.N. Lathiotakis)

ORCID(s): 0000-0003-2661-5743 (Z.G. Fthenakis);

0000-0002-5589-7930 (N.N. Lathiotakis)

the corresponding fullerene, by removing C atoms from the irreducible part of the triangles formed by the centers of neighboring pentagons in that fullerene. Then two-fold C atoms at the pore boundaries should be replaced by pyridinic N atoms. Maybe, other C atoms could be replaced by graphitic N atoms, as well, like in the design of $g-C_nN_m$ s. It is easy to show that C_{20} and C_{30} fullerenes of the $(n, 0)$ fullerene family (corresponding to the $(n, 0)$ Goldberg polyhedra), and C_{60} fullerene of the (n, n) fullerene family (corresponding to the (n, n) Goldberg polyhedra) can not be the precursors in the design of PCNFs. As a consequence, the smallest members of the $(n, 0)$ and (n, n) fullerene families that can be the precursors of PCNF design are C_{180} and C_{240} , respectively. The PCNFs derived from them are the $C_{60}N_{60}$ and $C_{120}N_{60}$, respectively, corresponding to the $g-CN$ and $g-C_2N$ 2D structures. These PCNFs ($C_{60}N_{60}$ and $C_{120}N_{60}$) together with the corresponding 2D structures ($g-CN$ and $g-C_2N$, respectively) are shown in Fig. 1. In the same figure, graphene and icosahedral C_{60} are also shown, to emphasize the relation between (i) graphene with C_{60} , (ii) graphene with $g-C_nN_m$ s, and (iii) icosahedral fullerenes with PCNFs.

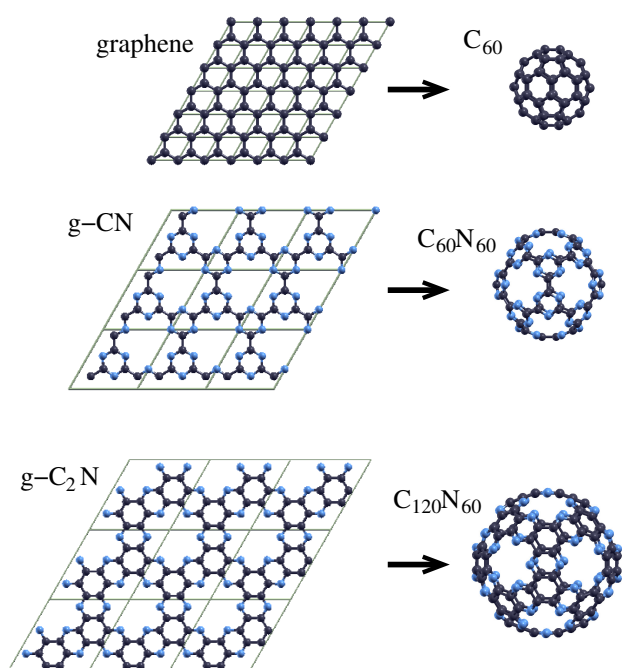


Figure 1: 2D structures (graphene and $g-C_nN_m$ s) and their fullerene counterparts.

In the present work, we theoretically study $C_{60}N_{60}$ and $C_{120}N_{60}$ as representatives of the PCNF family. We investigate their stability (including their formation energies) and their structural, vibrational, and electronic properties. Our findings reveal that both structures are dynamically, thermally, and electronically stable. Following the presentation of our theoretical results, we discuss the potential for bottom-up synthesis of PCNFs using possible precursors.

2. Methods

For the structural, vibrational, and electronic properties, we employ Density Functional Theory (DFT) with state-of-the-art functionals, namely the range-separated, hybrid ω B97X-D [34] and the hybrid meta-GGA MN15 [35], as implemented in the Gaussian 16 code [36]. For these calculations, the 6311-G(d,p) basis set was used, which was found appropriate for this study. The vibrational analysis certified that both PCNFs are dynamically stable structures. The ionization potentials (IPs) and electron affinities (EAs) were obtained as the absolute energy differences between the neutral molecule and positive and negative ions respectively. For the ions, separate calculations of the doublet states were performed, with full geometry relaxation. The large values of the obtained chemical hardness and HOMO-LUMO gaps demonstrate the stability of the electronic state of both PCNFs.

The formation energies of $C_{60}N_{60}$ and $C_{120}N_{60}$ were calculated using periodic DFT calculations with the PBE functional supplemented with Grimme's D3 dispersion corrections [37], as implemented in the Quantum Espresso code [38]. This methodology allows the treatment of the two molecules and their periodic 2D counterparts at the same level of theory and orbital expansion. We adopted the projected augmented wave method (and pseudopotentials) and kinetic energy cutoffs for the wavefunctions and the density 60 and 500 Ryd, respectively. For the periodic structures, $24 \times 24 \times 1$ k-mesh were used, while for the two molecules, Γ -point calculations were performed in a cubic supercell of a 36 \AA side.

Regarding thermal stability, molecular dynamics (MD) simulations were performed under NVT conditions, for $0 \leq T \leq 2000 \text{ K}$, with a 100 K increment, using the CHON-2019 [39] and the GR-RDX-2021 [40] ReaxFF potentials. For these simulations, the LAMMPS [41] suite was employed, the NVT conditions were simulated using the Nosé-Hoover thermostat [42, 43], and the time step adopted was 0.25 fsec, for all cases. First, an annealing simulation was performed, under NVT conditions, using 2×10^6 time steps, from 300 K down to 0 K, followed by a conjugate gradient optimization to find the energetically optimum structure. Before each NVT simulation at a specific temperature T , thermalization of the optimized structure at that T was performed, under NVT conditions, for 10^5 time steps. Following thermalization, 2×10^6 time steps of molecular dynamics simulation were performed, and the time average of the energy for each such simulation was calculated. Similar simulations were performed for C_{60} for comparison. These MD simulations reveal that $C_{60}N_{60}$ PCNF is stable well above 1000 K and $C_{120}N_{60}$ well above 2000 K.

3. Results and discussion

3.1. Equilibrium geometry and structural features

In Fig. 2, we show two different views for each of the equilibrium structures of $C_{60}N_{60}$ (panels (a)) and $C_{120}N_{60}$ (panel (b)). As we see, these two structures are composed

of C_3N_3 and C_4N_2 hexagons, respectively, interconnected with C-C bonds. In $C_{120}N_{60}$, these interconnecting bonds with the C-C bonds within C_4N_2 hexagons form hexagonal Carbon rings. The geometries of the structures are presented in the Supporting Information in Cartesian coordinates (xyz format).

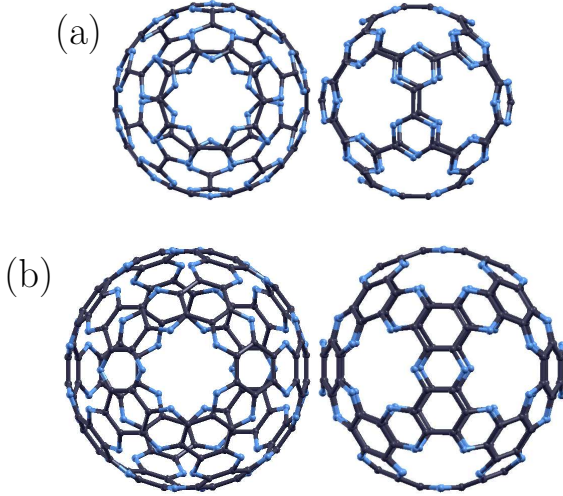


Figure 2: Structures of (a) $C_{60}N_{60}$ and (b) $C_{120}N_{60}$ from two different viewpoints. C atoms are shown in black and N atoms in blue.

As one can see in Fig. 1, these structural features of $C_{60}N_{60}$ and $C_{120}N_{60}$, as well as their stoichiometry, are identical with those in the g-CN and g- C_2N , respectively. The main morphological differences between the two PCNFs and their 2D counterparts are (i) the curvature of the PCNFs instead of the planarity of the g-CN and g- C_2N , and (ii) the pentagonal form of the pores in the two PCNFs instead of the hexagonal ones in the 2D structures. Considering an expansion of Fthenakis nomenclature scheme for graphene pores [44, 45], to include PCNFs, their pores are labeled as 33333, while those of the g-CN and g- C_2N as 333333. In comparison with the corresponding initial C_{180} and C_{240} C-fullerenes, the $C_{60}N_{60}$ and $C_{120}N_{60}$ PCNFs contain exclusively hexagonal rings, unlike C-fullerenes which contain also pentagons. Instead, they comprise those pentagonal 33333 pores.

The optimized geometries of the two PCNFs, obtained by our calculations with the ω B97X-D functional, are shown in Fig. 2. They are practically identical to those obtained with the MN15 functional, as seen in Tab. 1, where several structural properties of the two PCNFs are presented.

The C-C and C-N bond lengths in $C_{60}N_{60}$ were found to be $d_{C-C} \approx 1.52$ Å and $d_{C-N} \approx 1.33$ Å, respectively. The diameter of the pores, defined as the diameter of the circumscribed circle of the N-atoms pentagon is $D \approx 4.56$ Å. The triazine hexagons C_3N_3 are almost planar, with only a small elevation, $\delta d = 0.023$ Å, of the N-atoms plane, outwards with respect to that of the C-atoms plane. Considering the $C_{60}N_{60}$ as a sphere, its diameter, defined as the distance

between diametrically opposite C or N atoms, is $d_{C-C}^{sphere} \approx 11.3$ Å and $d_{N-N}^{sphere} \approx 11.4$ Å, respectively.

For the $C_{120}N_{60}$, two different kinds of C-C bonds exist: those interconnecting the C_4N_2 hexagons with length $d_{C-C} \approx 1.48$ Å, and those of the C_6N_2 hexagons with lengths $d'_{C-C} \approx 1.415$ Å. The length of the C-N bonds is $d_{C-N} \approx 1.33$ Å, as in the case of $C_{60}N_{60}$. The N-atoms elevation outwards is $\delta d \approx 0.66$ Å, almost three times larger than that of $C_{60}N_{60}$, although still small. The diameter D of the pores is $D \approx 4.565$ Å, i.e. practically the same as that of $C_{60}N_{60}$ pores. As expected, the corresponding sphere diameter is larger than that of $C_{60}N_{60}$ by approximately 2 Å, with values $d_{C-C}^{sphere} \approx 13.3$ Å and $d_{N-N}^{sphere} \approx 13.5$ Å.

For comparison, we performed optimization calculations for the icosahedral C_{60} fullerene with the same methods. According to our findings, the length of the common bonds of adjacent pentagons and hexagons (single bonds) is $d_{hp} \approx 1.45$ Å, and the length of the common bonds of adjacent hexagons (double bonds) is $d_{hh} \approx 1.39$ Å. These values are comparable with the d_{C-C} and d'_{C-C} bond lengths of $C_{60}N_{60}$ and $C_{120}N_{60}$, with $d_{C-C}^{C_{60}N_{60}} > d_{C-C}^{C_{120}N_{60}} > d_{hp}$ and $d'_{C-C} > d_{hh}$. This is a strong indication that the C-C bonds interconnecting C_3N_3 hexagons in $C_{60}N_{60}$ and C_4N_2 hexagons in $C_{120}N_{60}$ exhibit single bond character. Instead, those of the C_4N_2 hexagons have the character of a double bond. Moreover, it indicates that the C-C bonds of $C_{60}N_{60}$ and $C_{120}N_{60}$ are weaker than those of C_{60} , with those of $C_{120}N_{60}$ being stronger than those of $C_{60}N_{60}$.

Since the diameter D and the atomic environment of the pores for both $C_{60}N_{60}$ and $C_{120}N_{60}$ are practically the same, the molecular permeation properties of those pores are expected to be very similar. The local curvature is the only parameter that might differentiate these properties, varying between the two PCNFs due to their different sphere diameters. It is worth noting, that the size of the pore diameter is within the range of interesting pores for the permeation of small molecules [21–23, 25, 27]. We should mention that several members of the PCNF family, incorporate these pentagonal pores, which (to the best of our knowledge) have not been observed in any other structure, so far. On the other hand, such pentagonal pores might also exist as defects in g- C_nN_m s, modifying the structure and impairing its planarity locally. The properties related to such pores make these structures particularly interesting.

Molecular cage structures, like PCNFs, hold promise as traps for small molecules or metal clusters. Given the size of the radius of the PCNFs, one can expect that up to a few small molecules can be accommodated in these cages. Molecule trapping in these systems has the potential for a wide range of applications.

3.2. Electronic properties

Due to the icosahedral symmetry of the $C_{60}N_{60}$ and $C_{120}N_{60}$, the energy levels are in most cases degenerate. In particular, the HOMOs for the $C_{60}N_{60}$ and the $C_{120}N_{60}$ are five- and three-fold degenerate, respectively, while the

| Functional | $C_{60}N_{60}$ | | $C_{120}N_{60}$ | |
|--------------------|---------------------|--------|-----------------|--------|
| | ω B97X-D | MN15 | ω B97X-D | MN15 |
| d_{C-C} | 1.520 | 1.518 | 1.478 | 1.477 |
| d'_{C-C} | | | 1.413 | 1.417 |
| d_{C-N} | 1.327 | 1.330 | 1.325 | 1.328 |
| δd | 0.023 | 0.023 | 0.066 | 0.065 |
| D | 4.553 | 4.561 | 4.561 | 4.573 |
| d_{C-C}^{sphere} | 11.314 | 11.332 | 13.314 | 13.321 |
| d_{N-N}^{sphere} | 11.392 | 11.410 | 13.461 | 13.465 |
| IP | 9.20 | 9.23 | 8.56 | 8.08 |
| EA | 2.08 | 2.60 | 2.19 | 2.79 |
| η | 3.56 | 3.32 | 3.18 | 2.64 |
| HOMO | -9.73 | -8.68 | -8.65 | -7.61 |
| LUMO | -2.02 | -3.15 | -2.23 | -3.28 |
| H-L Gap | 7.71 | 5.53 | 6.42 | 4.32 |
| | Mulliken Population | | | |
| C atoms | 0.24 | 0.20 | 0.12 | 0.095 |
| N atoms | -0.24 | -0.20 | -0.24 | -0.19 |
| min. ν | 75.6 | 76.1 | 90.0 | 88.2 |

Table 1

Structural, electronic and vibrational features of $C_{60}N_{60}$ and $C_{120}N_{60}$ calculated utilizing the ω B97X-D and MN15 functionals and the 6-311G(d,p) basis set. All interatomic distances, energies, charges, and minimum frequencies (min. ν) are given in Å, eV, electrons, and cm^{-1} , respectively.

LUMOs are three- and five-fold degenerate, respectively. However, in both cases, the HOMO orbitals are fully occupied, enhancing stability, like the aromatic ring molecules.

The electron density corresponding to all five (for the $C_{60}N_{60}$) and all three (for the $C_{120}N_{60}$) degenerate HOMOs are shown in Fig. 3(a) and (b), respectively. As we see, they have entirely different characters. The HOMOs of $C_{60}N_{60}$ are dominated by Nitrogen sp^2 lone-pair states, while for $C_{120}N_{60}$, they have the character of p_{\perp} orbitals. With p_{\perp} we mean p-orbitals directed perpendicular to the $C_{120}N_{60}$ surface locally. Moreover, one can see that the HOMOs electron density for $C_{120}N_{60}$ is high along the C-C bonds of the C_4N_2 hexagons, indicating the presence of a double bond. Instead, along the C-C bonds interconnecting the C_4N_2 hexagons, it almost vanishes, in consistency with the presence of a single bond. We previously discussed the nature of these bonds concerning their length and the electron density plots confirm it. One can also see in Fig. 3(b) that the p_{\perp} contribution of N atoms is relatively small compared to that of the C atoms.

The LUMOs, on the other hand, are of p_{\perp} orbital character for both structures, as shown in Fig. 3(c) and (f), which depict one of the degenerate LUMOs of $C_{60}N_{60}$ and $C_{120}N_{60}$, respectively. Although not shown here, the other degenerate LUMOs have the same character differing mainly in their location. In Figs. 3, we show the total electron density of $C_{60}N_{60}$ and $C_{120}N_{60}$ for completeness.

Our findings on the nature of the HOMOs' and LUMOs' of $C_{60}N_{60}$ and $C_{120}N_{60}$ are very similar to those for the valence and conduction bands of g-CN and g- C_2N , respectively. For g-CN, the valence band consists of the sp^2 orbitals of the nitrogen atoms' lone-pair electrons, lying in

the structure's plane and localized on the nitrogen atoms. Instead, the conduction band is composed of p_z orbitals of the C and N atoms [24]. For the g- C_2N , the valence band is composed mainly of the p_z orbitals of the C atoms, with a smaller contribution from the p_z orbitals of the N atoms. Instead, the conduction band is composed of p_z orbitals, of the N atoms mainly [19].

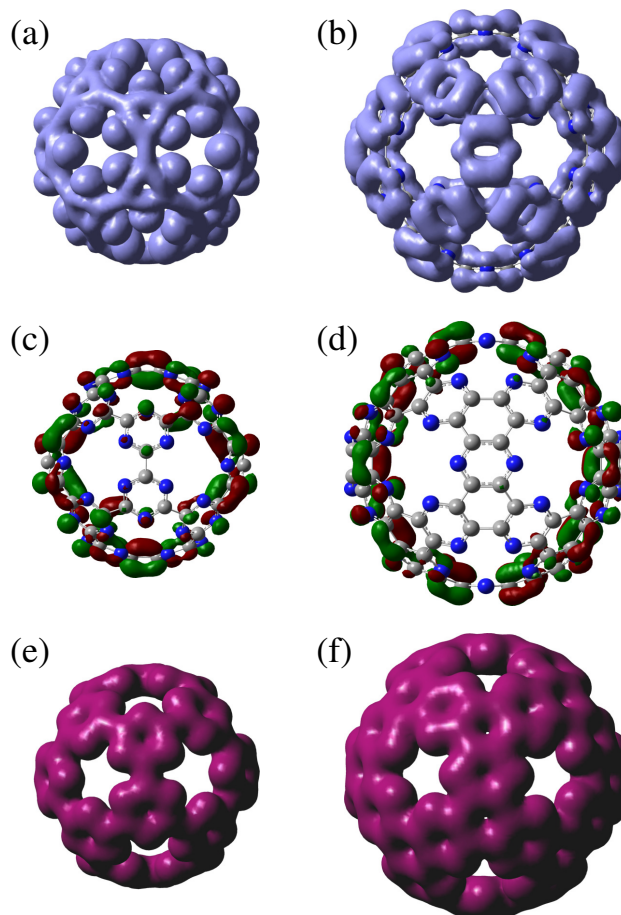


Figure 3: Electron density corresponding to all degenerate HOMOs of $C_{60}N_{60}$ (a) and $C_{120}N_{60}$ (b). One of the degenerate LUMOs of $C_{60}N_{60}$ (c) and $C_{120}N_{60}$ (d). Total electron density of $C_{60}N_{60}$ (e) and $C_{120}N_{60}$ (f).

For both structures, there is a relatively large HOMO - LUMO gap (H-L Gap) in comparison to the differences of the other successive energy levels of the occupied and unoccupied (virtual) orbitals, indicating a clear splitting between the π occupied states from the π^* unoccupied ones. The calculated HOMO, LUMO, and H-L gap values are shown in Tab. 1, together with the IP, EA, and chemical hardness, $\eta = (IP - EA)/2$. Notably, the HOMO and LUMO absolute values are good measures of IPs and EAs for the state-of-the-art approximations chosen. The large values of H-L gap and η strongly suggest that the electronic state of the studied PCNF structures is particularly stable. It is worth mentioning that, the EA values of PCNFs are large, like that of C_{60} , hence they could be promising candidates as electron

acceptors in several applications. The values of the IPs are also exceptionally large leading to large η .

For comparison, we also calculated the IP, EA, and H-L gap of C_{60} with $\omega B97X-D$ and MN15 functionals. We obtained IP=8.56, 8.01 eV, EA=2.32, 2.45 eV, and H-L Gap = 6.00, 3.92 eV, respectively. Thus, the chemical hardness for PCNFs is larger than that of C_{60} which is 2.84, 2.67 eV for $\omega B97X-D$ and MN15, respectively. The larger values of the H-L Gap and chemical hardness, compared to C_{60} , indicate that $C_{60}N_{60}$ and $C_{120}N_{60}$ are electronically more stable. The drop in the HOMO-LUMO gap from $C_{60}N_{60}$ to $C_{120}N_{60}$ seems to be similar to the behavior of the gap of graphene nanoribbons, which decreases as their width increases [46].

Furthermore, Mulliken population analysis reveals a weak charge transfer from N atoms to C atoms in both structures. Specifically, about 0.2 electrons move from each N atom and are equally distributed to the C atoms. Despite the charge transfer in the C-N bonds, the total dipole moment of PCNFs is zero, due to their icosahedral symmetry.

Regarding vibrational analysis, the results show that all eigenvalues of the dynamical matrix are positive (real vibrational frequencies), indicating dynamic stability. The minimum frequencies obtained are shown in Tab. 1 ($\nu_{min} \approx 76 \text{ cm}^{-1}$ for $C_{60}N_{60}$ and $\nu_{min} \approx 89 \text{ cm}^{-1}$ for $C_{120}N_{60}$). The corresponding minimum frequency value for C_{60} is $\nu_{min} \approx 266 \text{ cm}^{-1}$, indicating that C_{60} is dynamically more stable. This might be one of the reasons that according to MD simulations (see below), the fracture of PCNFs occurs at lower temperatures than C_{60} .

3.3. Formation energies of PCNFs

With the periodic DFT calculations described above, we calculated the formation energy per atom, $\Delta E^{(f)}$, of $C_{60}N_{60}$, $C_{120}N_{60}$ with respect to their 2D counterparts g-CN, g- C_2N , respectively. For comparison, we also calculated $\Delta E^{(f)}$ of Ih- C_{60} fullerene with respect to graphene. Using the calculated total energy E_{PCNF} of the PCNF and the total energy E_{2D} of its 2D counterpart per unit cell,

$$\Delta E^{(f)} = \frac{E_{PCNF}}{N_{PCNF}} - \frac{E_{2D}}{N_{2D}}, \quad (1)$$

where N_{PCNF} is the number of atoms of the PCNF and N_{2D} is the number of atoms in the unit cell of the corresponding 2D structure. We found that $\Delta E_{C_{60}N_{60}}^{(f)} = 0.09 \text{ eV/atom}$ and $\Delta E_{C_{120}N_{60}}^{(f)} = 0.08 \text{ eV/atom}$, while $\Delta E_{C_{60}}^{(f)} = 0.38 \text{ eV/atom}$. The small values of $\Delta E^{(f)}$ of $C_{60}N_{60}$ and $C_{120}N_{60}$ in comparison with that of C_{60} can be explained in terms of the large bond length deviations of C_{60} from the bond length of graphene ($d = 1.42 \text{ \AA}$), and the corresponding relatively large bond angle deviations of the pentagonal angles (108°) from the hexagonal ones of graphene (120°). The absence of pentagonal rings in $C_{60}N_{60}$ and $C_{120}N_{60}$ and the insignificant deviations of their bond lengths from the corresponding ones of g-CN and g- C_2N , respectively, significantly reduce the additional energy to form the PCNFs, which is mainly attributed to the strain energy due to the curvature.

| | | | |
|----------------|----------------|-----------------|----------|
| 0D | $C_{60}N_{60}$ | $C_{120}N_{60}$ | C_{60} |
| $E^{(f)}$ (eV) | 0.38 | 0.31 | 0.38 |
| 2D | g-CN | g- C_2N | graphene |
| $E^{(f)}$ (eV) | 0.29 | 0.23 | 0.00 |

Table 2

Calculated formation energies, $E^{(f)}$ with respect to graphene and N_2 molecule.

For completeness, we calculated the formation energies, $E^{(f)}$, of g-CN, g- C_2N , $C_{60}N_{60}$, $C_{120}N_{60}$, and Ih- C_{60} fullerene with respect to graphene and N_2 molecule, defined as

$$E^{(f)} = \frac{1}{N} \left[E - n_C \epsilon_g - n_N \epsilon_{N_2} \right] \quad (2)$$

where N is the number of atoms and E total energy of the PCNF, while n_C , n_N are the numbers of C and N atoms respectively, and ϵ_g , ϵ_{N_2} the total energies per atom of graphene and N_2 , respectively. The formation energies we obtained are listed in Tab. 2. As we see, the $E^{(f)}$ of $C_{60}N_{60}$ is approximately the same as that of C_{60} , while that of $C_{120}N_{60}$ is smaller. Also, that of g- C_2N is smaller than that of g-CN, which is unsurprising as this structure is ‘‘closer’’ to graphene with a larger density of hexagonal rings and less percentage of empty space.

3.4. Thermal stability

Figure 4 shows the time average of the energy E as a function of temperature T obtained from the MD simulations using the CHON-2019 and GR-RDX-2021 ReaxFFs for the $C_{60}N_{60}$ (left panels) and $C_{120}N_{60}$ (right panels). The linear relation between E and T at low temperatures represents the Dulong and Petit law, $E = 3Nk_B T$, which indicates the existence of a single phase. That phase is the ‘‘solid’’ state of the molecule. In the temperature range where this relation is valid, only atomic vibrations near the equilibrium positions occur. A divergence in the slope ($3Nk_B$) of the Dulong and Petit law indicates the initiation of a phase transition, usually accompanied by the coexistence of more phases. This phase transition finally leads to the fracture of the molecule. As shown in Fig. 4, the transition temperature for the $C_{60}N_{60}$ is well above 1000 K (1300 K for GR-RDX-2021 and 1600 K for CHON-2019) and for $C_{120}N_{60}$ well above 2000 K (2500 K for the GR-RDX-2021 and 2200 K for the CHON-2019). For comparison, we performed similar MD simulations for C_{60} with CHON-2019, and we found that the transition starts at around 3800 K. This value is in agreement with the work of Kim and Tománek [47], reporting a transition temperature between 3400 and 3800 K using tight-binding MD simulations. While the estimated transition temperatures and minimum vibration frequencies for $C_{60}N_{60}$ and $C_{120}N_{60}$ are lower than those of C_{60} , they are still sufficiently high, to guarantee that both $C_{60}N_{60}$ and $C_{120}N_{60}$ are thermally stable at temperatures exceeding substantially 1000 K and 2000 K, respectively.

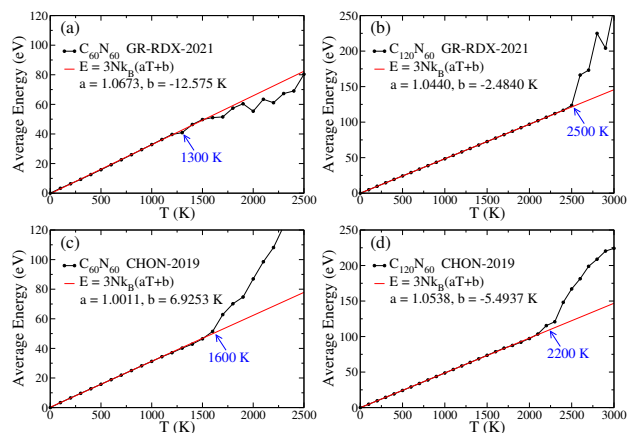


Figure 4: Average energy vs temperature obtained from MD simulations (i) using GR-RDX-2021 ReaxFF for $C_{60}N_{60}$ (a) and $C_{120}N_{60}$ (b), and (ii) using CHON-2019 ReaxFF for $C_{60}N_{60}$ (c) and $C_{120}N_{60}$ (d). For $C_{60}N_{60}$, $N = 120$ and for $C_{120}N_{60}$, $N = 180$. $k_B = 1/11604.5$ eV/K. The predicted temperatures at which the transition takes place are shown in blue.

3.5. On the feasibility of synthesizing $C_{60}N_{60}$ and $C_{120}N_{60}$

Although we found that both $C_{60}N_{60}$ and $C_{120}N_{60}$ are stable even at temperatures well above 1000 K and 2000 K, respectively, the most important issue is the existence of efficient routes for their synthesis. Likely, the most promising route involves bottom-up techniques, using proper precursors, similar to the synthesis of $g-C_nN_m$ s. Moreover, with proper nanosphere precursors including nitrogen functional groups, nitrogen-doped carbon nanospheres including pyridinic N atoms have already been synthesized [48]. Additionally, the synthesis of carbon nanospheres with $g-C_3N_4$ pores have also been reported [49, 50] as well as the synthesis of spherical carbon nitride nanostructures [51] with diameters ranging between 30 nm and 20 μ m. In similar experimental studies, the formation of hollow mesoporous carbon nitride microspheres has also been reported [52]. Therefore, the reported synthesis of both 2D $g-C_nN_m$ membranes [4, 9, 20, 53, 54] and carbon nanospheres [55, 56] as well as the minimal difference in the calculated formation energies of PCNFs compared to their 2D counterparts provide strong evidence for the feasibility of PCNF synthesis.

A possible precursor for the synthesis of $C_{60}N_{60}$ could be the 1,3,5-Triazinane ($C_3H_9N_3$), or the 1,3,5-Triazine, also called s-Triazine ($C_3H_3N_3$), or similar structures, like melamine ($C_3H_6N_6$) or cyanuric chloride ($C_3N_3Cl_3$). Cyanuric chloride has been involved (a) together with melamine in the synthesis of 2D $g-C_3N_4$ [57], (b) in the synthesis of carbon nitrogen nanotubes [58], as well as (c) the formation of CN nanotube bundles, nanoribbons, and microspheres [8] with 1:1 stoichiometry [59]. It is worth noting that one of the synthetic routes of the 2D $g-C_3N_4$ uses Cyanuric Chloride and melamine [57]. Moreover, the synthesis of the three star-shaped 1,3,5-Triazine derivatives [60] is also very promising.

A possible precursor for the synthesis of $C_{120}N_{60}$ could be (i) either Pyrazine ($C_4H_4N_2$), or 1,2-Dihydropyrazine ($C_4H_4(NH)_2$), or similar molecules which include the C_4N_2 hexagon, or (ii) 1,3,5-Benzenetriamine ($C_6H_3(NH_2)_3$), or 1,3,5-Trinitrobenzene ($C_6H_3(NO_2)_3$), or similar molecules, which include the C_6 hexagon with three bonded N atoms. The synthesis of Pyrazinacenes [61] based on Pyrazine may be a good starting point. Moreover, it is very promising for the synthesis of $C_{120}N_{60}$ the synthesis of its 2D counterpart, $g-C_2N$, via (a) a bottom-up wet-chemical reaction, using the precursors hexaaminobenzene trihydrochloride and hexaketocyclohexane octahydrate [5] and (b) polymerization of hexaaminobenzene (precursor), produced using amination of chloroanilic acid [6], (c) eutectic syntheses using as precursors the cyclohexanehexone and urea [7]. Other synthetic methods for $g-C_2N$ have been also reported [4].

We should note that this work is purely theoretical and the discussion in the present section provides simply some arguments supporting the possibility of PCNF synthesis. Synthesis, however, is definitely beyond the scope of the present work.

4. Conclusions

In this study, we present a novel family of structures, the porous carbon nitride fullerenes, representing the zero-dimensional analog of the two-dimensional porous carbon nitrides, just as fullerenes can be seen as the zero-dimensional counterparts of graphene. Our study focuses on the first members of that family of structures with icosahedral symmetry, (namely the $C_{60}N_{60}$ and $C_{120}N_{60}$), which are derived from the class I and II Goldberg polyhedra, respectively, following the two C_N icosahedral fullerene subfamilies with $N = 20n^2$, (C_{20} subfamily) and $N = 60n^2$, (C_{60} subfamily), $n = 1, 2, 3, \dots$, respectively.

We performed DFT calculations with two state-of-the-art functionals (ω B97X-D and MN15) and determined the optimal geometrical properties, the HOMO and LUMO energies and the vibrational frequencies of $C_{60}N_{60}$ and $C_{120}N_{60}$. We also determined their IPs and EAs as absolute total energy differences of the neutral structures from the positive and negative ions, respectively. We found that $C_{60}N_{60}$ and $C_{120}N_{60}$ are dynamically stable, while the large values of the H-L gap and chemical hardness indicate a robust electronic state. Due to their large EAs, these molecules could be used as electron acceptors. The two structures have 12 identical N-terminated pentagonal-like pores each, with practically equal pore diameter ($D \approx 4.56$ Å), which is in the diameter range of the interesting pores for the permeation of small molecules and they can capture metallic atoms for catalytic applications. The unique features of the pentagonal-like pores and the particular features rising from the cage shape of those molecules make them potentially interesting for several applications well beyond the applications of their 2D counterparts.

Moreover, we performed molecular dynamics simulations under NVT conditions with the CHON-2019 and GR-RDX-2021 ReaxFFs, and we showed that the $C_{60}N_{60}$ and $C_{120}N_{60}$ PCNFs are thermally stable well above 1000 K and 2000 K, respectively. Additionally, we discuss possible precursors, which could be used in a bottom-up synthesis of these structures. We expect the new proposed molecules to be of great importance after their synthesis, as porous molecules, in trapping small molecules, and in catalysis.

Acknowledgments

ZGF acknowledges financial support from the project PRIN 2022 - Cod. 202278NHAM (PE11) CHERICH-C “Chemical and electrochemical energy storage materials from organic wastes: the treasure hidden in C-based materials” - CUP B53D23008590006, funded by the European Union – Next Generation EU in the context of the Italian National Recovery and Resilience Plan, Mission 4, Component 2, Investment 1.1, “Fondo per il Programma Nazionale di Ricerca e Progetti di Rilevante Interesse Nazionale (PRIN)”.

NNL acknowledges support by the framework of the Action “Flagship Research Projects in challenging interdisciplinary sectors with practical applications in Greek Industry”, implemented through the National Recovery and Resilience Plan Greece 2.0 and funded by the European Union - NextGenerationEU (Acronym: 3GPV-4INDUSTRY, project code: TAEDR-0537347).

References

- [1] H. Montigaud, B. Tanguy, G. Demazeau, I. Alves, and S. Courjault. C_3N_4 : Dream or reality? Solvothermal synthesis as macroscopic samples of the C_3N_4 graphitic form. *J. Mater. Sci.*, 35:2547–2552, 2000. doi: 10.1023/A:1004798509417. URL <https://doi.org/10.1023/A:1004798509417>.
- [2] Xinchun Wang, Kazuhiko Maeda, Xiufang Chen, Kazuhiro Takanabe, Kazunari Domen, and Yidong et al. Hou. Polymer semiconductors for artificial photosynthesis: Hydrogen evolution by mesoporous graphitic carbon nitride with visible light. *J. Am. Chem. Soc.*, 131(5):1680–1681, 2009. doi: 10.1021/ja809307s. URL <https://doi.org/10.1021/ja809307s>.
- [3] Pawan Kumar, Ehsan Vahidzadeh, Ujwal K. Thakur, Piyush Kar, Kazi M. Alam, and Ankur et al. Goswami. C_3N_5 : A low bandgap semiconductor containing an azo-linked carbon nitride framework for photocatalytic, photovoltaic and adsorbent applications. *J. Am. Chem. Soc.*, 141(13):5415–5436, 2019. doi: 10.1021/jacs.9b00144. URL <https://doi.org/10.1021/jacs.9b00144>.
- [4] Li Tan, Chunyang Nie, Zhimin Ao, Hongqi Sun, Taicheng An, and Shaobin Wang. Novel two-dimensional crystalline carbon nitrides beyond g- C_3N_4 : structure and applications. *J. Mater. Chem. A*, 9:17–33, 2021. doi: 10.1039/D0TA07437C. URL <http://dx.doi.org/10.1039/D0TA07437C>.
- [5] Javed Mahmood, Eun Kwang Lee, Minbok Jung, Dongbin Shin, In-Yup Jeon, and Sun-Min et al. Jung. Nitrogenated holey two-dimensional structures. *Nat. Commun.*, 6:6486, 2015. doi: 10.1038/ncomms7486. URL <https://doi.org/10.1038/ncomms7486>.
- [6] Sambhaji S. Shinde, Chi Ho Lee, Jin-Young Yu, Dong-Hyung Kim, Sang Uck Lee, and Jung-Ho Lee. Hierarchically designed 3D holey C_2N aerogels as bifunctional oxygen electrodes for flexible and rechargeable zn-air batteries. *ACS Nano*, 12(1):596–608, 2018. doi: 10.1021/acsnano.7b07473. URL <https://doi.org/10.1021/acsnano.7b07473>.
- [7] Nina Fechner, Niels P. Zussblatt, Regina Rothe, Robert Schlögl, Marc-Georg Willinger, and Bradley F. et al. Chmelka. Eutectic syntheses of graphitic carbon with high pyrazinic nitrogen content. *Adv. Mater.*, 28(6):1287–1294, 2016. doi: <https://doi.org/10.1002/adma.201501503>. URL <https://onlinelibrary.wiley.com/doi/abs/10.1002/adma.201501503>.
- [8] Jie Li, Chuanbao Cao, Jianwei Hao, Hailin Qiu, Yajie Xu, and Hesun Zhu. Self-assembled one-dimensional carbon nitride architectures. *Diamond Relat. Mater.*, 15(10):1593–1600, 2006. doi: <https://doi.org/10.1016/j.diamond.2006.01.013>. URL <https://www.sciencedirect.com/science/article/pii/S092596350600240>.
- [9] Cora Moreira Da Silva, Maxime Vallet, Clément Semion, Thomas Blin, Romuald Saint-Martin, and Jocelyne et al. Leroy. A simple and efficient process for the synthesis of 2D carbon nitrides and related materials. *Sci. Rep.*, 13:15423, 2023. doi: 10.1038/s41598-023-39899-5. URL <https://doi.org/10.1038/s41598-023-39899-5>.
- [10] H. J. Xiang, B. Huang, Z. Y. Li, S.-H. Wei, J. L. Yang, and X. G. Gong. Ordered semiconducting nitrogen-graphene alloys. *Phys. Rev. X*, 2:011003, Jan 2012. doi: 10.1103/PhysRevX.2.011003. URL <https://link.aps.org/doi/10.1103/PhysRevX.2.011003>.
- [11] Yongyong Cao, JinYan Zhao, Xing Zhong, Guilin Zhuang, Shengwei Deng, and Zhongzhe Wei et al. Building highly active hybrid double-atom sites in C_2N for enhanced electrocatalytic hydrogen peroxide synthesis. *Green Energy & Envir.*, 6(6):846–857, 2021. doi: <https://doi.org/10.1016/j.gee.2020.12.006>. URL <https://www.sciencedirect.com/science/article/pii/S2468025720302417>.
- [12] Xinmiao Liu and Li Sheng. Al-embedded C_2N : a DFT study on a promising catalyst for CO oxidation. *New J. Chem.*, 46:9250–9257, 2022. doi: 10.1039/D1NJ05689A. URL <http://dx.doi.org/10.1039/D1NJ05689A>.
- [13] B. L. He, J. S. Shen, and Z. X. Tian. Iron-embedded C_2N monolayer: a promising low-cost and high-activity single-atom catalyst for CO oxidation. *Phys. Chem. Chem. Phys.*, 18:24261–24269, 2016. doi: 10.1039/C6CP03398A. URL <http://dx.doi.org/10.1039/C6CP03398A>.
- [14] Qing Han, Nan Chen, Jing Zhang, and Liangti Qu. Graphene/graphitic carbon nitride hybrids for catalysis. *Mater. Horiz.*, 4:832–850, 2017. doi: 10.1039/C7MH00379J. URL <http://dx.doi.org/10.1039/C7MH00379J>.
- [15] Yuwen Cheng, Yan Song, and Yumin Zhang. A systematic investigation of the catalytic performances of monolayer carbon nitride nanosheets $C_{1-x}N_x$. *Phys. Chem. Chem. Phys.*, 22:6772–6782, 2020. doi: 10.1039/D0CP00319K. URL <http://dx.doi.org/10.1039/D0CP00319K>.
- [16] Shengyang Su, Junmei Ma, Zhenhua Liu, Domoina Holiharmanana, and Hao Sun. Catalytic reduction of N_2O by CO on single-atom catalysts Au/ C_2N and Cu/ C_2N : A first-principles study. *Catalysts*, 13(3):578, 2023. doi: 10.3390/catal13030578. URL <https://www.mdpi.com/2073-4344/13/3/578>.
- [17] M.R. Ashwin Kishore, Anja Olafsen Sjøstad, and P. Ravindran. Influence of hydrogen and halogen adsorption on the photocatalytic water splitting activity of C_2N monolayer: A first-principles study. *Carbon*, 141:50–58, 2019. doi: <https://doi.org/10.1016/j.carbon.2018.08.072>. URL <https://www.sciencedirect.com/science/article/pii/S0008622318308078>.
- [18] Huimin Wang, Xingxing Li, and Jinlong Yang. The g- C_3N_4/C_2N nanocomposite: A g- C_3N_4 -based water-splitting photocatalyst with enhanced energy efficiency. *ChemPhysChem*, 17(13):2100–2104, 2016. doi: <https://doi.org/10.1002/cphc.201600209>. URL <https://chemistry-europe.onlinelibrary.wiley.com/doi/abs/10.1002/cphc.201600209>.
- [19] M. R. Ashwin Kishore and Ponniah Ravindran. Tailoring the electronic band gap and band edge positions in the C_2N monolayer by p and as substitution for photocatalytic water splitting. *J. Phys. Chem. C*, 121(40):22216–22224, 2017. doi: 10.1021/acs.jpcc.7b07776. URL <https://doi.org/10.1021/acs.jpcc.7b07776>.
- [20] Guilherme F. S. R. Rocha, Marcos A. R. da Silva, Andrea Rogolino, Gabriel A. A. Diab, Luis F. G. Noleto, and Markus et al. Antonietti.

- Carbon nitride based materials: more than just a support for single-atom catalysis. *Chem. Soc. Rev.*, 52:4878–4932, 2023. doi: 10.1039/D2CS00806H. URL <http://dx.doi.org/10.1039/D2CS00806H>.
- [21] Yong-Chao Rao, Zhao-Qin Chu, Xiao Gu, and Xiang-Mei Duan. Theoretical design of a strain-controlled nanoporous cn membrane for helium separation. *Comput. Mater. Sci.*, 161:53–57, 2019. doi: <https://doi.org/10.1016/j.commatsci.2019.01.017>. URL <https://www.sciencedirect.com/science/article/pii/S0927025619300205>.
- [22] Yuanyuan Qu, Feng Li, Hongcai Zhou, and Mingwen Zhao. Highly efficient quantum sieving in porous graphene-like carbon nitride for light isotopes separation. *Sci. Rep.*, 6:19952, 2016. doi: 10.1038/srep19952. URL <https://doi.org/10.1038/srep19952>.
- [23] Yuanyuan Qu, Feng Li, and Mingwen Zhao. Efficient hydrogen isotopologues separation through a tunable potential barrier: The case of a C₂N membrane. *Sci. Rep.*, 7:1483, 2017. doi: 10.1038/s41598-017-01488-8. URL <https://doi.org/10.1038/s41598-017-01488-8>.
- [24] Zhengzheng Chen, Pengfei Li, and Chao Wu. A uniformly porous 2D CN (1:1) network predicted by first-principles calculations. *RSC Adv.*, 5:11791–11796, 2015. doi: 10.1039/C4RA15322G. URL <http://dx.doi.org/10.1039/C4RA15322G>.
- [25] Lei Zhu, Qingzhong Xue, Xiaofang Li, Tiantian Wu, Yakang Jin, and Wei Xing. C₂N: an excellent two-dimensional monolayer membrane for He separation. *J. Mater. Chem. A*, 3:21351–21356, 2015. doi: 10.1039/C5TA05700K. URL <http://dx.doi.org/10.1039/C5TA05700K>.
- [26] Xiao Chang, Lei Zhu, Qingzhong Xue, Xiao Li, Tianchao Guo, and Xiaofang Li et al. Charge controlled switchable CO₂/N₂ separation for g-C₁₀N₉ membrane: Insights from molecular dynamics simulations. *J. CO₂ Utiliz.*, 26:294–301, 2018. doi: <https://doi.org/10.1016/j.jcou.2018.05.017>. URL <https://www.sciencedirect.com/science/article/pii/S2212982018301720>.
- [27] Xueshi Wei, Zhiyong Liu, Qihua Hou, Xuehan Zhang, Zihao Wang, and Ruishan Zhang et al. Theoretical design of an effective he separation membrane based on nanoporous C₉N₄ monolayer. *J. Indust. Eng. Chem.*, 131:329–336, 2024. doi: <https://doi.org/10.1016/j.jiec.2023.10.032>. URL <https://www.sciencedirect.com/science/article/pii/S1226086X23006524>.
- [28] You-sheng Yu, Rong-ri Tan, and Hong-ming Ding. Controlling ion transport in a C₂N-based nanochannel with tunable interlayer spacing. *Phys. Chem. Chem. Phys.*, 22:16855–16861, 2020. doi: 10.1039/D0CP02993A. URL <http://dx.doi.org/10.1039/D0CP02993A>.
- [29] Mohammad Mehrdad and Ali Moosavi. Novel adjustable monolayer carbon nitride membranes for high-performance saline water desalination. *Nanotechnology*, 32(4):045706, oct 2020. doi: 10.1088/1361-6528/abb6a6. URL <https://dx.doi.org/10.1088/1361-6528/abb6a6>.
- [30] Puspamitra Panigrahi, Manish Desai, Murali Krishna Talari, Hyeonhu Bae, Hoonkyung Lee, and Rajeev Ahuja et al. Selective decoration of nitrogenated holey graphene (C₂N) with titanium clusters for enhanced hydrogen storage application. *Int. J. Hydrogen Energy*, 46(10):7371–7380, 2021. doi: <https://doi.org/10.1016/j.ijhydene.2020.11.222>. URL <https://www.sciencedirect.com/science/article/pii/S0360319920344724>.
- [31] Jiantie Xu, Javeed Mahmood, Yuhai Dou, Shixue Dou, Feng Li, and Liming et al. Dai. 2D frameworks of C₂N and C₃N as new anode materials for lithium-ion batteries. *Adv. Mater.*, 29(34):1702007, 2017. doi: <https://doi.org/10.1002/adma.201702007>. URL <https://onlinelibrary.wiley.com/doi/abs/10.1002/adma.201702007>.
- [32] Michael Goldberg. A class of multi-symmetric polyhedra. *Tohoku Math. J., First Series*, 43:104–108, 1937.
- [33] R. Bruce King and Mircea V. Diudea. The chirality of icosahedral fullerenes: a comparison of the tripling (leapfrog), quadrupling (chamfering), and septupling (capra) transformations. *J. Math. Chem.*, 39:597–604, 2006. doi: 0.1007/s10910-005-9048-7. URL <https://doi.org/10.1007/s10910-005-9048-7>.
- [34] Jeng-Da Chai and Martin Head-Gordon. Long-range corrected hybrid density functionals with damped atom–atom dispersion corrections. *Phys. Chem. Chem. Phys.*, 10:6615–6620, 2008. doi: 10.1039/B810189B. URL <http://dx.doi.org/10.1039/B810189B>.
- [35] Haoyu S. Yu, Xiao He, Shaohong L. Li, and Donald G. Truhlar. MN15: A Kohn–Sham global-hybrid exchange–correlation density functional with broad accuracy for multi-reference and single-reference systems and noncovalent interactions. *Chem. Sci.*, 7:5032–5051, 2016. doi: 10.1039/C6SC00705H. URL <http://dx.doi.org/10.1039/C6SC00705H>.
- [36] M. J. Frisch, G. W. Trucks, H. B. Schlegel, G. E. Scuseria, M. A. Robb, and J. R. Cheeseman et al. Gaussian–16 Revision C.01, 2016. Gaussian Inc. Wallingford CT.
- [37] Stefan Grimme, Jens Antony, Stephan Ehrlich, and Helge Krieg. A consistent and accurate ab initio parametrization of density functional dispersion correction (DFT-D) for the 94 elements H–Pu. *J. Chem. Phys.*, 132(15):154104, 04 2010. doi: 10.1063/1.3382344. URL <https://doi.org/10.1063/1.3382344>.
- [38] P Giannozzi, O Andreussi, T Brumme, O Bunau, M Buongiorno Nardelli, and M Calandra et al. Advanced capabilities for materials modelling with Quantum ESPRESSO. *J. Phys.: Cond. Matter*, 29(46):465901, oct 2017. doi: 10.1088/1361-648X/aa8f79. URL <https://dx.doi.org/10.1088/1361-648X/aa8f79>.
- [39] Malgorzata Kowalik, Chowdhury Ashraf, Behzad Damirchi, Dooman Akbarian, Siavash Rajabpour, and Adri C. T. van Duin. Atomistic scale analysis of the carbonization process for C/H/O/N-based polymers with the reaxff reactive force field. *J. Phys. Chem. B*, 123(25):5357–5367, 2019. doi: 10.1021/acs.jpcc.9b04298. URL <https://doi.org/10.1021/acs.jpcc.9b04298>.
- [40] Zacharias G. Fthenakis, Ioannis D. Petsalakis, Valentina Tozzini, and Nektarios N. Lathiotakis. Evaluating the performance of ReaxFF potentials for sp² carbon systems (graphene, carbon nanotubes, fullerenes) and a new reaxff potential. *Front. Chem.*, 10:951261, 2022. doi: 10.3389/fchem.2022.951261. URL <https://www.frontiersin.org/articles/10.3389/fchem.2022.951261>.
- [41] Aidan P. Thompson, H. Metin Aktulga, Richard Berger, Dan S. Bolintineanu, W. Michael Brown, and Paul S. Crozier et al. LAMMPS - a flexible simulation tool for particle-based materials modeling at the atomic, meso, and continuum scales. *Comp. Phys. Commun.*, 271:108171, 2022. doi: <https://doi.org/10.1016/j.cpc.2021.108171>. URL <https://www.sciencedirect.com/science/article/pii/S0010465521002836>.
- [42] Shuichi Nosé. A unified formulation of the constant temperature molecular dynamics methods. *J. Chem. Phys.*, 81(1):511–519, 07 1984. doi: 10.1063/1.447334. URL <https://doi.org/10.1063/1.447334>.
- [43] William G. Hoover. Canonical dynamics: Equilibrium phase-space distributions. *Phys. Rev. A*, 31:1695–1697, Mar 1985. doi: 10.1103/PhysRevA.31.1695. URL <https://link.aps.org/doi/10.1103/PhysRevA.31.1695>.
- [44] Zacharias G. Fthenakis. A proposed nomenclature for graphene pores: a systematic study of their geometrical features and an algorithm for their generation and enumeration. *Carbon*, 199:508–519, 2022. doi: <https://doi.org/10.1016/j.carbon.2022.07.038>. URL <https://www.sciencedirect.com/science/article/pii/S0008622322005632>.
- [45] Zacharias G. Fthenakis. A generalized nomenclature scheme for graphene pores, flakes, and edges, and an algorithm for their generation and numbering. *Nanomaterials*, 13(16):2343, 2023. doi: 10.3390/nano13162343. URL <https://www.mdpi.com/2079-4991/13/16/2343>.
- [46] Young-Woo Son, Marvin L. Cohen, and Steven G. Louie. Energy gaps in graphene nanoribbons. *Phys. Rev. Lett.*, 97:216803, Nov 2006. doi: 10.1103/PhysRevLett.97.216803. URL <https://link.aps.org/doi/10.1103/PhysRevLett.97.216803>.
- [47] Seong Gon Kim and David Tománek. Melting the fullerenes: A molecular dynamics study. *Phys. Rev. Lett.*, 72:2418–2421, Apr 1994. doi: 10.1103/PhysRevLett.72.2418. URL <https://link.aps.org/doi/10.1103/PhysRevLett.72.2418>.
- [48] Hu Zhang, Jingkun Hu, Yongchuan Liu, Changxin Lin, Xiangxin Zhang, and Yining Zhang. Nitrogen-doped carbon nanospheres for capacitive deionization. *ACS Appl. Nano Mater.*, 6(24):22956–22967, 2023. doi: 10.1021/acsnm.3c04289. URL <https://doi.org/10.1021/acsnm.3c04289>.

- [49] Qianqian Song, Junqi Li, Lei Wang, Lingyan Pang, and Hui Liu. Controlling the chemical bonding of highly dispersed co atoms anchored on an ultrathin g-C₃N₄@carbon sphere for enhanced electrocatalytic activity of the oxygen evolution reaction. *Inorg. Chem.*, 58(16): 10802–10811, 2019. doi: 10.1021/acs.inorgchem.9b01089. URL <https://doi.org/10.1021/acs.inorgchem.9b01089>.
- [50] Yihua Tang, Xiao Wang, Jingjing Chen, Xinxin Wang, Dajian Wang, and Zhiyong Mao. Templated transformation of g-C₃N₄ nanosheets into nitrogen-doped hollow carbon sphere with tunable nitrogen-doping properties for application in Li-ions batteries. *Carbon*, 168:458–467, 2020. doi: <https://doi.org/10.1016/j.carbon.2020.07.022>. URL <https://www.sciencedirect.com/science/article/pii/S0008622320306825>.
- [51] John L. Zimmerman, Robert Williams, Valery N. Khabashesku, and John L. Margrave. Synthesis of spherical carbon nitride nanostructures. *Nano Lett.*, 1(12):731–734, 2001. doi: 10.1021/nl015626h. URL <https://doi.org/10.1021/nl015626h>.
- [52] Jian Li, Lin Han, Xinxin Ye, Min Zhang, Yueyue Hu, and Tao Jiang. Facile fabrication of hollow carbon nitride microspheres with mesoporous structures: When ethanol meets cyanamide. *Particuology*, 53:186–191, 2020. ISSN 1674-2001. doi: <https://doi.org/10.1016/j.partic.2020.02.007>. URL <https://www.sciencedirect.com/science/article/pii/S1674200120300432>.
- [53] T. S. Miller, A. Belen Jorge, T. M. Suter, A. Sella, F. Corà, and P. F. McMillan. Carbon nitrides: synthesis and characterization of a new class of functional materials. *Phys. Chem. Chem. Phys.*, 19:15613–15638, 2017. doi: 10.1039/C7CP02711G. URL <http://dx.doi.org/10.1039/C7CP02711G>.
- [54] Chun-Yao Wang, Kazuhiko Maeda, Lee-Lee Chang, Kuo-Lun Tung, and Chechia Hu. Synthesis and applications of carbon nitride (CN_x) family with different carbon to nitrogen ratio. *Carbon*, 188:482–491, 2022. doi: <https://doi.org/10.1016/j.carbon.2021.12.027>. URL <https://www.sciencedirect.com/science/article/pii/S0008622321011866>.
- [55] Jian Liu, Shi Zhang Qiao, Hao Liu, Jun Chen, Ajay Orpe, and Dongyuan et al. Zhao. Extension of the Stöber method to the preparation of monodisperse resorcinol–formaldehyde resin polymer and carbon spheres. *Angew. Chem. Int. Ed.*, 50(26):5947–5951, 2011. doi: <https://doi.org/10.1002/anie.201102011>. URL <https://onlinelibrary.wiley.com/doi/abs/10.1002/anie.201102011>.
- [56] Zheng-Guang Liu, Xiang-Xi He, Jia-Hua Zhao, Chun-Mei Xu, Yun Qiao, Li Li, and Shu-Lei Chou. Carbon nanosphere synthesis and applications for rechargeable batteries. *Chem. Commun.*, 59:4257–4273, 2023. doi: 10.1039/D3CC00402C. URL <http://dx.doi.org/10.1039/D3CC00402C>.
- [57] Zhao Zhang, Si Wu, Jian Zhang, Shunxi Tang, Chunyuan Hu, and Yingai et al. Li. Well-aligned carbon nitride nanorods: the template-free synthesis and their optical and thermal properties. *Appl. Phys. A*, 119:1507–1513, 2015. doi: 10.1007/s00339-015-9128-x. URL <https://doi.org/10.1007/s00339-015-9128-x>.
- [58] Sonja Tragl, Katharina Gibson, Jochen Glaser, Viola Duppel, Arndt Simon, and H.-Jürgen Meyer. Template assisted formation of micro- and nanotubular carbon nitride materials. *Solid State Commun.*, 141(9):529–534, 2007. doi: <https://doi.org/10.1016/j.ssc.2006.10.008>. URL <https://www.sciencedirect.com/science/article/pii/S0038109806009148>.
- [59] Chuanbao Cao, Fulin Huang, Chuantang Cao, Jie Li, and Hesun Zhu. Synthesis of carbon nitride nanotubes via a catalytic-assembly solvothermal route. *Chem. Mater.*, 16(25):5213–5215, 2004. doi: 10.1021/cm0493039. URL <https://doi.org/10.1021/cm0493039>.
- [60] Hsiao-Fan Chen, Shang-Jung Yang, Zhen-Han Tsai, Wen-Yi Hung, Ting-Chih Wang, and Ken-Tsung Wong. 1,3,5-triazine derivatives as new electron transport-type host materials for highly efficient green phosphorescent oleds. *J. Mater. Chem.*, 19:8112–8118, 2009. doi: 10.1039/B913423A. URL <http://dx.doi.org/10.1039/B913423A>.
- [61] Gary J. Richards, Jonathan P. Hill, Toshiyuki Mori, and Katsuhiko Ariga. Putting the ‘N’ in acene: Pyrazinacenes and their structural relatives. *Org. Biomol. Chem.*, 9:5005–5017, 2011. doi: 10.1039/